Cerebral Cortex March 2010;20:602-611
doi:10.1093/cercor/bhp127
Advance Access publication June 26, 2009

Spatial Distribution of Deep Sulcal Landmarks and Hemispherical Asymmetry on the Cortical Surface

Kiho Im[1], Hang Joon Jo[2], Jean-François Mangin[3], Alan C. Evans[4], Sun I. Kim[1] and Jong-Min Lee[1]

[1]Department of Biomedical Engineering, Hanyang University, Seoul 133-791, South Korea, [2]Scientific and Statistical Computing Core, National Institute of Mental Health, National Institutes of Health, Department of Health and Human Services, Bethesda, MD 20892-1148, USA, [3]LNAO, Neurospin, I2BM, CEA, 91190 Gif-sur-Yvette, France and [4]McConnell Brain Imaging Centre, Montreal Neurological Institute, McGill University, Montreal, QC, Canada H3A 2B4

The locally deepest regions of major sulci, the sulcal pits, are thought to be the first cortical folds to develop and are closely related to functional areas. We examined the spatial distribution of sulcal pits across the entire cortical region, and assessed the hemispheric asymmetry in their frequency and distribution in a large group of normal adult brains. We automatically extracted sulcal pits from magnetic resonance imaging data using surface-based methods and constructed a group map from 148 subjects. The spatial distribution of the sulcal pits was relatively invariant between individuals, showing high frequency and density in specific focal areas. The left and right sulcal pits were spatially covariant in the regions of the earliest developed sulci. The sulcal pits with great spatial invariance appear to be useful as stable anatomical landmarks. We showed the most significant asymmetry in the frequency and spatial variance of sulcal pits in the superior temporal sulcus, which might be related to the lateralization of language function to the left hemisphere, developing more consistently and strongly than for the right. Our analyses support previous empirical and theoretical studies, and provide additional insights concerning the anatomical and functional development of the brain.

Keywords: brain development, cortical folding, functional lateralization, magnetic resonance imaging, sulcal pits

Introduction

The pattern of sulcal and gyral folds, the principal anatomical landmarks of the human cerebral cortex, exhibits structural complexity and large intersubject variability. Understanding the spatial relationships between structure and functional features, and the precise anatomical correspondence across different brains, remains a challenge. Although the origin and meaning of this variability are still unclear, the first cortical folds to develop appear to be stable in number, position, and orientation (Regis et al. 1995, 2005; Cachia et al. 2003; Lohmann et al. 2008). These may therefore be used as stable anatomical landmarks for matching different cortical folding patterns between subjects. The formation of the first sulci occurs during the early stage of radial growth of the cerebral cortex, and their formation may be closely related to functional areas and the protomap of cytoarchitectonic areas (Rakic 1988; Hasnain et al. 2001; Regis et al. 2005; Lohmann et al. 2008). The sulci that form later during the tangential growth of the cerebral cortex appear to be more variable, both in appearance and in their relationship to functional areas (Hasnain et al. 2001, 2006). It is therefore important to identify those sulcal landmarks (the putative first cortical folds) that form early and that retain their identity during development in the human brain. Moreover, their spatial distribution may be important for understanding the anatomical and functional development of the human brain.

Brain asymmetry has been observed in humans in terms of structure, function, and behavior. The left hemisphere is normally dominant for language and logical processing, whereas the right hemisphere is involved in spatial recognition (Riss 1984; Geschwind and Miller 2001). The distribution of human brain function between the left and right hemispheres is associated with asymmetries in anatomical structures such as the Sylvian fissures (SFs), planum temporale, and superior temporal regions (Good et al. 2001; Sowell et al. 2002; Ochiai et al. 2004; Van Essen 2005). This lateralized specialization may arise from evolutionary, developmental, genetic, experiential, or pathological factors (Toga and Thompson 2003). Asymmetrical gene expression in the human embryonic cortex appears as early as 12 weeks (Sun et al. 2005; Sun and Walsh 2006). If the sulci that form early are related to functional areas and the formation is under genetic control (Lohmann et al. 1999, 2008), their appearance and spatial distribution should be asymmetrical and associated with lateralized brain function.

The locally deepest regions of sulci, called the *sulcal pits*, are the first to develop and subsequently change the least as the cortex expands (Lohmann et al. 2008). The sulcal pits previously described had a regular spatial arrangement and showed less variation between individuals than the more superficial cortical regions. However, that study used a volume image and was confined to the lateral brain areas because of limitations in the methods used (Lohmann et al. 2008). The first cortical folds were called *sulcal roots*, and a multiscale-based representation of the sulcal folding patterns was used to identify putative sulcal roots on a cortical surface model of the adult brain (Cachia et al. 2003). These putative sulcal roots were recovered from the curvature of the surface in the sulcal fundic regions. However, these results were confined to one of the simplest sulci, the central sulcus (CS), in a few subjects, and the spatial distribution pattern and intersubject variability were not described. To the best of our knowledge, there has not been an examination of the hemispheric asymmetry of these sulcal landmarks.

We examined the spatial distribution of the deep sulcal landmarks (assumed to be the first cortical folds in the adult brain) across the entire cortical region, and assessed the hemispheric asymmetry in their frequency and distribution in a large group of normal adult brains. We considered that the sulcal pits, the locally deepest points of a sulcal fundus (Lohmann et al. 2008), are the significant sulcal landmarks. We identified sulcal pits using the cortical surface obtained from magnetic resonance imaging (MRI) data.

Materials and Methods

Data Acquisition

This study used the data set of the International Consortium for Brain Mapping that has been used in many previous studies (Mazziotta et al. 1995; Watkins et al. 2001; Im, Lee, Lyttelton, et al. 2008). The subjects scanned were 152 unselected normal volunteers. Each subject gave written informed consent and the Research Ethics Committee of the Montreal Neurological Institute (MNI) and Hospital approved the study. Each subject was scanned using a Phillips Gyroscan 1.5 T superconducting magnet system. The sequence that was used yielded T_1-weighted images (3-dimensional [3D] fast field echo scan with 140–160 slices, 1-mm isotropic resolution, time repetition [TR] = 8 ms, time echo [TE] = 0 ms, flip angle = 30°). We excluded 4 subjects from the 152 because of surface modeling errors. The final sample consisted of 83 men and 65 women. Their ages ranged from 18 to 44 years (mean ± standard deviation: 25.0 ± 4.9 years). As determined from a short questionnaire, 15 subjects were left-handed on a number of tasks and 124 subjects preferred to use their right hand. The hand-dominance for 9 subjects was not known.

Image Processing and Cortical Surface Extraction

Images were processed using a standard MNI anatomical pipeline. The native images were normalized to a standardized stereotaxic space using a linear transformation and corrected for intensity nonuniformity (Collins et al. 1994; Sled et al. 1998). The registered and corrected volumes were classified into white matter, gray matter, cerebrospinal fluid, and background using an advanced neural-net classifier (Zijdenbos et al. 1996). The hemispherical surfaces of the inner and outer cortex, consisting of 40 962 vertices, were automatically extracted using the Constrained Laplacian-Based Automated Segmentation with Proximities algorithm (MacDonald et al. 2000; Kim et al. 2005). We used the inner cortical surface to extract the sulcal landmarks.

Sulcal Depth

Sulcal depth maps were generated by measuring the 3D Euclidean distance from each vertex in the inner cortical surface to the nearest voxel on the cerebral hull. This approach has been employed and described in our previous studies (Im, Lee, Lyttelton, et al. 2008; Im, Lee, Seo, et al. 2008). We masked the surfaces to the images, isolated inner voxels of the surfaces and binarized the images to extract the cerebral hull volume. We performed a 3D morphological closing operation on the binarized image using a structuring element of spherical shape. The radius of the structuring element was 10 mm, which is larger than the maximum radius of the sulcus. We detected the edge of the image with the Laplacian of the Gaussian mask and constructed a cerebral hull volume that wrapped around the hemisphere, but did not encroach into the sulci.

Extraction of Sulcal Pits on the Cortical Surface

A sulcal pit is the deepest point in a sulcal catchment basin, and it can be identified by using the structural information of small gyri buried in depths of sulci called *plis de passage* (the focal elevation of the sulcal bottom) (Gratiolet 1854; Regis et al. 2005). The *plis de passage*, which was described as the remnant of the development of separate sulcal segments (Cunningham 1905), is located between 2 sulcal pits within a sulus. We used a watershed algorithm to extract the locally deepest points of the sulci on triangular meshes. The concept underlying our watershed processing has been previously described (Rettmann et al. 2002; Yang and Kruggel 2008). The algorithm initially sorts the depth values and creates a list of vertices that are ordered by their depth. The vertex of the largest depth was first defined as the sulcal pit, the initial vertex of a catchment basin. If the next vertex in the list was the neighbor of the previously identified catchment basin, it was added to this catchment basin. If all of its neighbors were unlabeled, we created a new sulcal pit as a seed vertex for the next catchment basin. A vertex can touch more than one existing catchment basin, and that vertex is a ridge point where growing catchment basins join. In this case, the vertex would be assigned to the closest catchment basin. This processing was terminated when the depth of the vertex in the list was less than a threshold value of 7 mm. This threshold was chosen to avoid detecting unimportant pits that belonged to small, shallow sulci.

The original cortical surfaces had noisy features and small geometric variations in shape, and therefore their sulcal depth maps were not smooth. The watershed algorithm applied to the original sulcal depth map overextracted sulcal pits because of small, noisy ridges and catchment basins (Fig. 1). Surface-based diffusion smoothing with a full-width half-maximum (FWHM) value of 10 mm was used to smooth the depth maps (Chung et al. 2003). Although smoothing with the 10-mm kernel was not enough to eliminate all noise, larger kernels may remove not only noise, but also true sulcal pits. The results of the watershed algorithm using different smoothing kernels are shown in Figure 1. Our methods resulted in a slight overextraction of the pits rather than underextraction. Instead of using a larger smoothing kernel, we removed noisy sulcal pits by merging processing as described following.

(a) Our first merging criterion was based on the areas of the catchment basins. Noisy catchment basins for minor local variations have small areas. If 1 of the areas of 2 or more catchment basins was smaller than a threshold when they met at a ridge point, the smaller catchment basin below the threshold was merged into the adjacent catchment basin with the deepest pit and its sulcal pit was removed. We empirically set the threshold at 30 mm^2. We calculated the Voronoi region area of each vertex for local surface area (Meyer et al. 2002). The area of any arbitrary region on a triangular mesh can be measured as the sum of the Voronoi areas of the vertices making up that region (Fig. 2*A*).

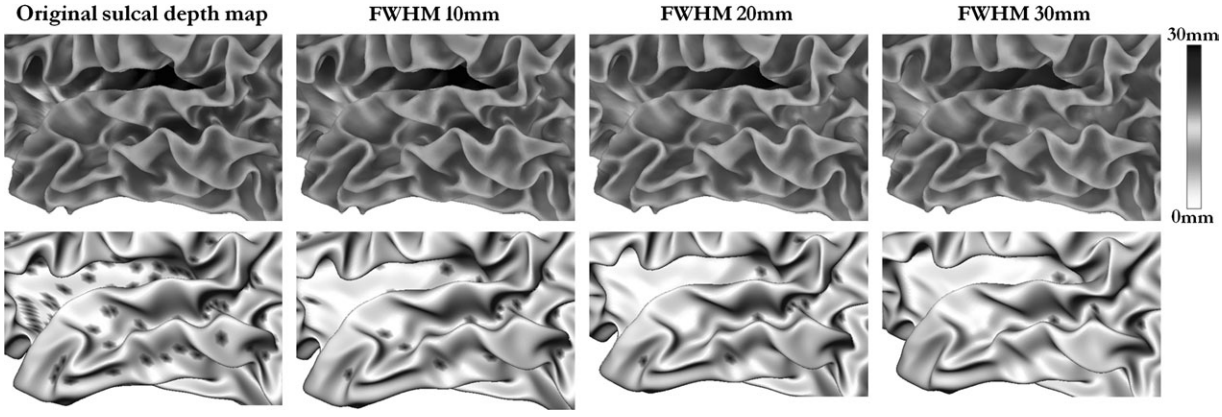

Figure 1. Sulcal pit extraction using the watershed algorithm applied to sulcal depth maps with different kernels of diffusion smoothing for an individual cortical surface. The top row in the figure shows the depth maps of the left temporal area with increases in the smoothing kernel from 0 to 30 mm. The sulcal-pit maps based on these depth maps are shown in the second row. Sulcal pits were heavily overextracted in the original sulcal depth map. In the smoothed map at FWHM 20 mm, noisy pits were removed, but they were still present in the middle region of the STS. Some true sulcal pits seem absent on the map with smoothing at FWHM 30 mm.

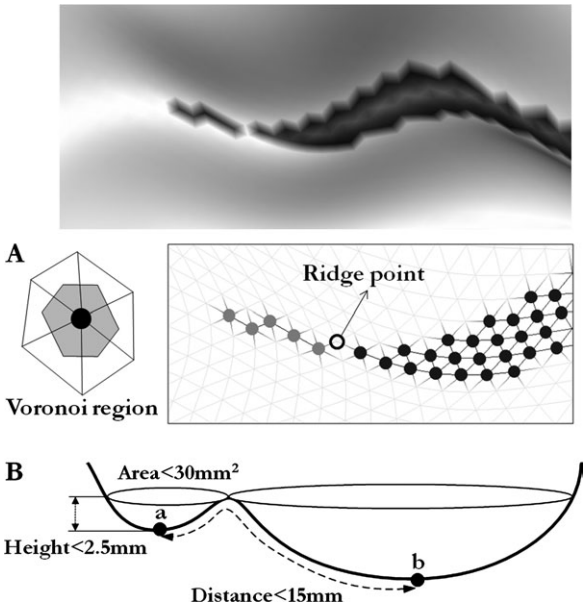

Figure 2. Merge processing in the watershed algorithm. This example shows the meeting of 2 catchment basins at a ridge point during watershed processing. The area of the catchment basin on triangular meshes was measured using the Voronoi region area of the vertices (*A*). The schematic illustration of merging criteria is shown. The sulcal pit *a* was merged into *b* if (area < 30 mm^2 or distance < 15 mm) and (height < 2.5 mm) (*B*).

(b) We merged some sulcal pits using a second criterion, the distance between the pits. We computed the geodesic distance along the surface from all sulcal pits as seed vertices (Lanthier et al. 2001; Robbins 2003; Robbins et al. 2004). If the distance between any 2 pits was less than a 15 mm threshold, the shallower pit was merged into the deeper one. This criterion is based on the assumption that early, deep sulcal points may not be very close to each other. Previous studies describing the clusters of sulcal pits and the generic model of sulcal roots demonstrated that the distance from one location to another is larger than the 15 mm threshold that we used (Regis et al. 2005; Lohmann et al. 2008).

(c) The final criterion was that the height of the ridge (the depth of the sulcal pit minus the depth of the ridge) should be less than the threshold for merging. Although 1 of the 2 criteria described above was met, merging was not executed and the sulcal pit was considered to be present if the ridge was higher than a threshold of 2.5 mm. Thus the logic for merging required ((a OR b) AND c) (Fig. 2*B*). The same threshold value of ridge height for merging was previously used in a watershed algorithm to segment anatomically different sulci (Yang and Kruggel 2008).

Cluster Segmentation in the Group Map

Each individual map of sulcal pits was transformed to a surface group template using a 2-dimensional (2D) surface-based registration that aligns variable sulcal folding patterns through sphere-to-sphere warping (Robbins et al. 2004; Lyttelton et al. 2007). The surface group template is an unbiased, high-resolution iterative registration template from a group of 222 subjects' hemispheres (Lyttelton et al. 2007). The transformed pits from many subjects were located on the common template space and clustered at several specific regions. We segmented and defined clusters from the distribution of the pits, and classified each pit into the one of the clusters. First, the pits were smoothed with an FWHM of 10 mm, maintaining a peak value of 1 (Fig. 3*A*) (Chung et al. 2003). The smoothed pits from all subjects were overlaid on the template and their values were summed. Several regions of high density were shown in the group map of the smoothed pits, indicating that the sulcal pits from many subjects were clustered into these small regions (Fig. 3*B*). We segmented the cluster regions and detected the densest points (local maxima) in the clusters by using the watershed algorithm with the merging criterion of the area of the catchment basin described above. The area threshold was set as 30 mm^2 to avoid oversegmentation. Regions of low density whose values were less than 3 were excluded from running the watershed segmentation process. The improved surface registration algorithm and the group template with its increased anatomical detail (Lyttelton et al. 2007) allowed us to include some well-matched minor sulcal folds, and the sulcal pits of such folds were clustered in the group map. We manually selected the clusters located in the deep major sulci and excluded others because we were interested in the deep sulcal pits of major sulci that are related to early brain development. Pits occupying the same cluster had the same identity. If more than one pit was present in a cluster in one subject, the pit that was closest to the densest point was chosen for analysis.

Construction of a Local Coordinate System

Because the cortical surface starts from a spherical polygon model, the vertices can be inversely transformed to the spherical model (Kim et al. 2005). The sulcal pits, previously transformed to the common space of the surface template, can be distributed in a 2D spherical coordinate system. However, the spherical coordinates (θ, φ) of the pits cannot be used to calculate the shape distribution directly (Tao et al. 2002). We constructed a tangent plane as a local coordinate system for each cluster. On the tangent plane, we defined an orthogonal coordinate system (u, v) whose origin was the average position of the pits on the sphere. The pits of all subjects were then projected onto the tangent plane (Fig. 4). The methodological details have been described previously (Tao et al. 2002). We performed all data analyses based on the local coordinate system.

Data Analysis

The Frequency and Density of Sulcal Pits

We examined the frequency of sulcal pits. The percentage of subjects that had a pit in each cluster region was calculated (the number of pits (N_p)/148 × 100). This reflects the consistency of their appearance between subjects. We measured the density to assess the consistency of spatial localization of the pits within a sulcus. This density was defined as the percentage of pits present within a radius of 5 mm geodesic distance from each point of maximal density (the number of pits in the area of radius 5 mm (N_{p5})/N_p × 100).

Statistical Tests to Measure Hemispheric Asymmetry

We analyzed the hemispheric differences in data distribution. First, pit frequency asymmetry between left and right hemispheres was estimated using a χ^2 test. The presence of pits was modeled in the form of binary categorical variables taken to be 1 when the pits were present and 0 when absent. The variables for the left and right sides are also categorical. We generated crosstab table, relating 2 categorical variables with each other. A χ^2 test was used to see if there is a relationship between 2 categorical variables, or they appear to be independent. If the values in the cells of the table are not balanced, it means that the frequency of sulcal pits is asymmetric and dependent on the side. In those cases where the assumption of the χ^2 test (expected frequency of 5 or more in each cell) was not met, we adopted Fisher's exact test.

	Presence (1)	Absence (0)	
Left	*a* (frequency)	*b*	$a + b$ (148)
Right	*c*	*d*	$c + d$ (148)
	$a + c$	$b + d$	

$$\chi^2 = \frac{(ad - bc)^2 (a + b + c + d)}{(a + b)(c + d)(b + d)(a + c)}$$

Second, we tested the differences in spatial variance of the pits between the left and right hemispheres. An equality of variance was

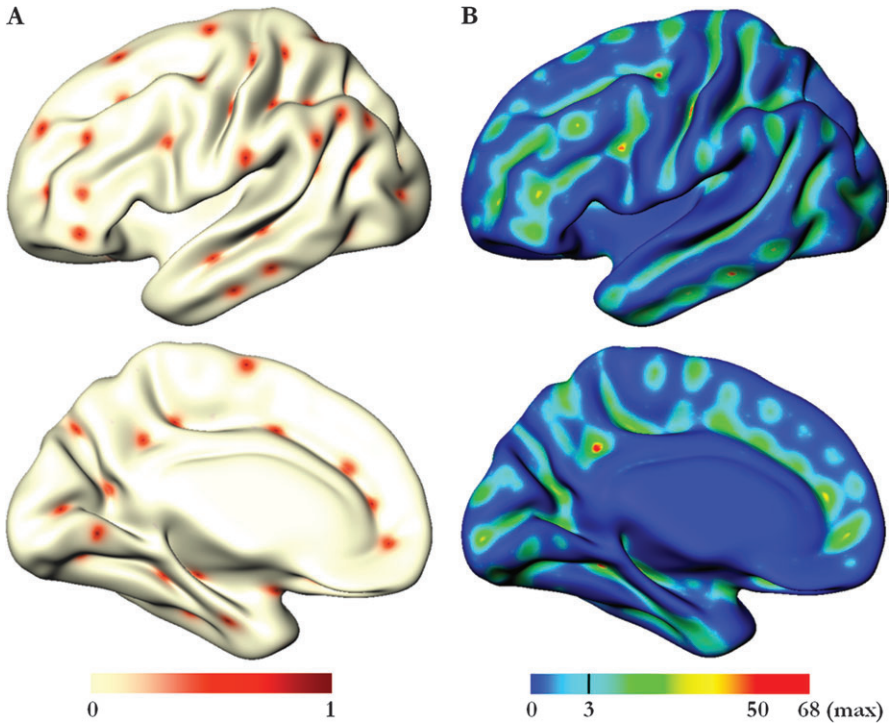

Figure 3. The sulcal pits extracted from an individual were transformed to the surface group template and smoothed with an FWHM of 10 mm, maintaining the peak value of 1 (*A*). The group map was constructed by overlaying all individual maps of the smoothed pits and summing their values (*B*). Several areas of high density, shown in yellow and red, can be seen, indicating the clustering of sulcal pits from many subjects in specific regions.

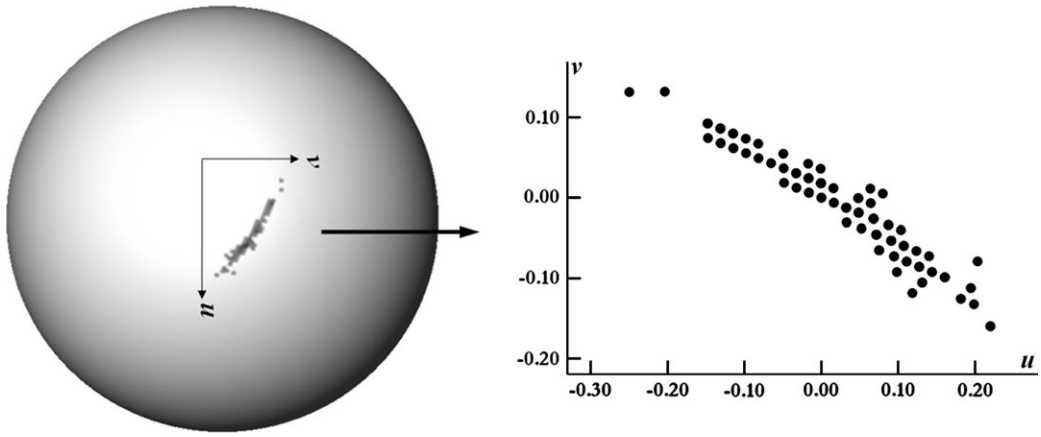

Figure 4. Sulcal pits on a spherical coordinate system were projected onto the tangent plane as a local coordinate system. On the tangent plane, we define an orthogonal coordinate system (*u*, *v*) with the origin taken as the average position of the pits on the sphere.

assessed using Levene's test (Levene 1960). Third, we examined the differences in the spatial distribution of the pits between the hemispheres. Because measurements made in the left and right hemispheres are dependent on each other, the differences in the multiple variables (*u*, *v*) were tested using a repeated-measures multivariate analysis of variance (MANOVA), with side (left and right) entered as the within-subject variable.

Spatial Covariance of Sulcal Pits between Left and Right Hemispheres

We investigated covariance in the location of sulcal pits on the template surface between the hemispheres. The spatial covariance between the left and right pits was assessed using a canonical correlation analysis. This is a multivariate statistical technique for describing and quantifying correlated variation between sets of vector variables (the *u* and *v* in our study). A canonical correlation analysis has been used to quantify the correlated behavior of different subcortical structures (Rao et al. 2008).

Results

We applied our method of sulcal pit extraction to MRI data from 148 normal adult brains. The final individual maps of sulcal pits and sulcal catchment basins are shown in Figure 5. The data in the first column on the left in Figure 5 show the same subject as in Figure 1. Any noisy pits remaining after applying diffusion smoothing were eliminated using merging, leaving only the likely pits on the left temporal lobe. Figure 6 shows the final map of the segmented cluster regions extracted from

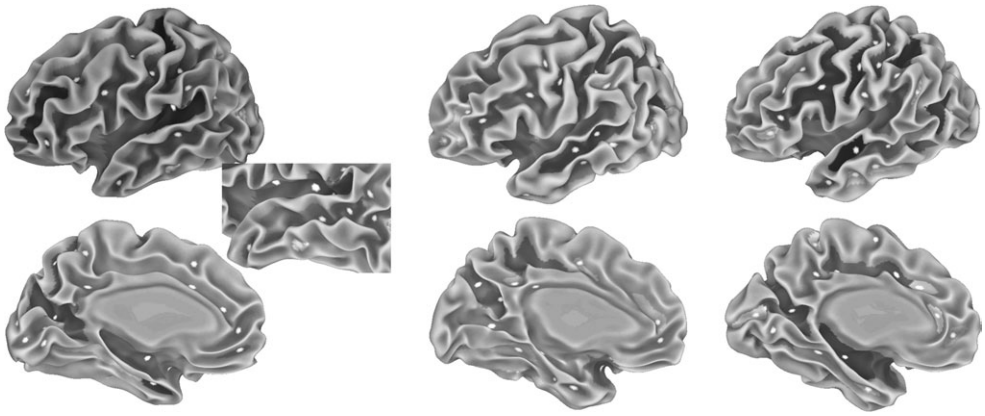

Figure 5. Final results of sulcal pit extraction in 3 subjects. The maps show the sulcal pits (white points) and the sulcal catchment basins on the cortical surfaces. The sulcal pit extraction on the left temporal lobe shown in the first column on the left can be compared with the results shown in Figure 1.

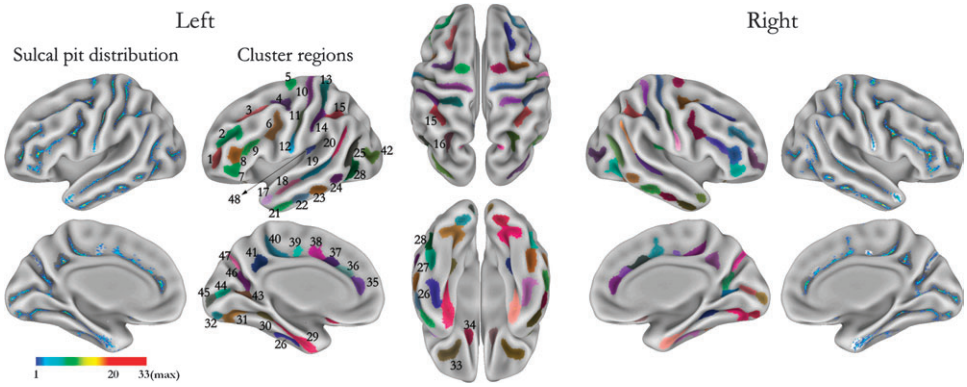

Figure 6. Final map of the segmented cluster regions and the distribution of sulcal pits belonging to major sulci. Forty-eight and 47 (due to the absence of cluster 18) clusters are shown in the left and right hemispheres, respectively. The clusters are labeled with numbers corresponding to the anatomical labels (s.: sulcus, 1 middle frontal s. a, 2 middle frontal s. b, 3 superior frontal s., 4 junction between superior frontal s. and precentral s., 5 precentral s., 6 junction between precentral s. and inferior frontal s., 7 inferior frontal s. a, 8 inferior frontal s. b, 9 inferior frontal s. c, 10 central s. a, 11 central s. b, 12 central s. c, 13 postcentral s. a, 14 postcentral s. b, 15 intraparietal s. a, 16 intraparietal s. b, 17 superior temporal s. a, 18 superior temporal s. b, 19 superior temporal s. c, 20 superior temporal s. d, 21 inferior temporal s. a, 22 inferior temporal s. b, 23 inferior temporal s. c, 24 inferior temporal s. d, 25 inferior temporal s. e, 26 occipito-temporal s. a, 27 occipito-temporal s. b, 28 occipito-temporal s. c, 29 collateral s. a, 30 collateral s. b, 31 collateral s. c, 32 collateral s. d, 33 orbital s., 34 olfactory s., 35 cingulate s. a, 36 cingulate s. b, 37 cingulate s. c, 38 cingulate s. d, 39 cingulate s. e, 40 cingulate s. f, 41 subparietal s., 42 lateral occipital s., 43 calcarine s. a, 44 calcarine s. b, 45 calcarine s. c, 46 parieto-occipital s. a, 47 parieto-occipital s. b, 48 SF).

the group of smoothed sulcal pits shown in Figure 3*B*, including the distribution of sulcal pits in the major sulci. Over the entire cortical region, 48 clusters were detected on the left hemisphere and 47 on the right. The frequency of pits was too low to form a significant cluster in the right middle region of the superior temporal sulcus (STS). A neuroanatomist assigned anatomical labels to the clusters based on the literature (Duvernoy 1991) (Fig. 6). Most major sulci contained 2–4 sulcal pit clusters. The inferior temporal sulcus (ITS) and the cingulate sulcus (CiS) have long, variable shapes and contained more than 4 sulcal pit clusters. There was only one cluster for some of the sulci (orbital sulcus [OrS], olfactory sulcus, subparietal sulcus [SPS], lateral occipital sulcus, and SF). The areas of sulcal pit clusters were nearly symmetrical in both hemispheres, except for one region. Note that the cluster in STS *b* was not present in the right hemisphere. The region of this cluster in the left hemisphere was masked and applied to the homologous area in the right hemisphere for asymmetry analyses.

The results of the frequency calculation showed that a high percentage of subjects had a sulcal pit within each cluster. Almost every subject possessed a sulcal pit within the SF cluster region with 99% and 100% for the left and right hemispheres, respectively. Other cluster regions with a frequency of more than 90% were the right middle frontal sulcus (MFS) *a*, the superior frontal sulcus (SFS) and postcentral sulcus (PoCS) *b*, both (left and right) MFS *b*, the junction between SFS and precentral sulcus (PrCS), the junction between PrCS and inferior frontal sulcus (IFS), CS *a* and *b*, intraparietal sulcus (IPS) *b*, STS *c*, ITS *e*, collateral sulcus (CoS) *b*, OrS, CiS *f*, SPS, and parieto-occipital sulcus (POS) *a*. The density of pits in some of these clusters was high, with a high proportion of pits lying within a 5 mm radius. The densities were higher than 70% in the clusters in the left IPS *b*, right MFS *a* and PoCS *b*, and both (left and right) the junction between SFS and PrCS, the junction between PrCS and IFS, CS *b*, CoS *b*, and SPS. The frequency and density of all pits are shown in supplementary material.

Statistical tests were performed for each cluster region to determine asymmetry. The statistics were conservatively set to a significance threshold of $P = 0.001$ ($\fallingdotseq 0.05/48$) using Bonferroni correction. A χ^2 test showed that the number of the pits in the left hemisphere was significantly larger than in

the right hemisphere for the regions in PoCS *a* (left/right: 114/87, χ^2 = 11.30, P = 0.0008), STS *b* (60/19, χ^2 = 29.03, P < 0.0001) and *d* (128/81, χ^2 = 35.96, P < 0.0001), and calcarine sulcus (CaS) *a* (115/83, χ^2 = 15.62, P < 0.0001). The POS *b* region had a significantly larger number of pits in the right hemisphere than in the left (35/72, χ^2 = 20.04, P < 0.0001). The most significant difference in pit frequency between the hemispheres was seen in the STS. The clusters in the STS also showed significant hemispheric differences in the spatial distribution of the pits. In the STS *d*, there was statistically significant asymmetry in the spatial variance of the pits in the cluster in the *v* variable of the local coordinate system ($F_{1,207}$ = 14.08, P = 0.0002) and a trend toward significance was shown in the *u* variable ($F_{1,207}$ = 7.52, P = 0.006). The spatial variance of the pits in the right hemisphere was greater than in the left. The distribution of the pits on the local coordinate system is shown in the scatter plot (Fig. 7*A*). There was no statistically significant asymmetry in the spatial variance in other clusters. The difference in the position of pit distribution between the 2 hemispheres for the STS *c* region (Fig. 8*A*) had the highest statistical significance ($F_{2,133}$ = 30.03, P < 0.0001) when tested using a repeated-measures MANOVA. This difference between the hemispheres was also statistically significant for the clusters in OrS ($F_{2,139}$ = 15.27, P < 0.0001), CiS *f* ($F_{2,144}$ = 7.75, P = 0.001), and POS *a* ($F_{2,125}$ = 23.34, P < 0.0001).

A canonical correlation analysis showed that the sulcal pits in the left and right hemispheres were spatially covariant in some of the major sulci. Highly significant spatial correlations were found for the clusters in the CS *b* (R = 0.430, P < 0.0001), SF (R = 0.569, P < 0.0001), CaS *a* (R = 0.534, P = 0.0005), and POS *a* (R = 0.349, P < 0.0001).

Discussion

We are the first to automatically extract and map sulcal pits across the entire cortical region using the surface model. Our method provides a surface-mesh–based procedure that is not prone to overextraction and therefore appears to detect true sulcal pits more reliably. The smoothing and merging criteria operate cooperatively and are important in detecting appropriate sulcal pits. We observed the intrinsic variability of sulcal pits along the sulcal valley in a 2D surface-based coordinate system, reducing the variability due to the 3D position, direction, and length of the sulcus. Methodological considerations are more explained in supplementary material.

Spatial Distribution, Frequency, and Density of Sulcal Pits

We constructed a group map of sulcal pits from 148 MRI data sets from normal adults and examined their spatial distribution. The major pattern of the distribution and organization of sulcal pits was analyzed by segmenting and identifying sulcal pit clusters associated with the major sulci. Forty-eight clusters were identified in the left hemisphere and 47 in the right hemisphere with most major sulci containing 2 or more clusters. Our results support previous studies in terms of the number and location of such clusters. Based on the anatomical and embryological literature, the CS is considered to consist of 2 primitive folds (Cachia et al. 2003; Regis et al. 2005). Imaging studies extracting putative sulcal roots and volume-based sulcal pits and substructures have described 2 regions in the CS (Lohmann and von Cramon 2000; Cachia et al. 2003; Lohmann et al. 2008). We found more than 95% of sulcal pits in the superior (CS *a*) and middle (CS *b*) part of the CS with positions corresponding to the positions of the sulcal roots (Cachia et al. 2003). The sulcal pits were clustered in the inferior part (CS *c*) of the CS in our map. This may be a consequence of using an advanced surface registration algorithm that matched individual sulcal folding patterns with high accuracy. However, the frequency in the CS *c* was quite low (less than 30%) and the area of this cluster was small in both hemispheres. The sulcal pit in the inferior CS is not major and may appear as a small fold in a few subjects. The presence of 4 sulcal roots and basins has been reported in the STS (Lohmann and von Cramon 2000; Cachia et al. 2003). Four sulcal pit clusters were present in the left STS, consistent with previous reports. However, we observed only 3 clusters in the right STS. The hemispheric asymmetry in the pattern of sulcal pits is discussed in detail in the following section. Our results are consistent with a previous sulcal root analysis in which the ITS contained 5 sulcal roots (Regis et al. 2005). We found that the PrCS and PoCS contained 3 and 2 pit clusters, respectively, in both hemispheres. This is also consistent with a previous study of sulcal basin extraction (Lohmann and von Cramon 2000). These observations confirm that our sulcal pit extraction and cluster maps are meaningful and interesting. Our pit cluster map can be used to automatically label sulcal pits extracted from other individual brains by matching them with a surface registration template.

The frequency and density of sulcal pits showed a consistency between subjects in the appearance and spatial location in each cluster. We found that there were several specific cluster regions showing a high frequency of sulcal pits. According to the radial unit hypothesis, the ventricular zone consists of proliferative units that form a protomap of cytoarchitectonic areas (Rakic 1988). The protomap model proposes that the cells in the embryonic cerebral vesicle carry intrinsic programs for species-specific cortical regionalization (Rakic 1988, 2001; Miyashita-Lin et al. 1999; Fukuchi-Shimogori and Grove 2001). Genetic control has an effect on the protomap and cortical regionalization, and is important in the development and distribution of cortical convolutions (Rubenstein and Rakic 1999; Piao et al. 2004; Rakic 2004). The gyrogenesis theory suggests that areas of rapid growth form gyri at the center of a functional zone, and boundaries between functional areas will tend to lie along the sulcal fundi (Welker 1990). The process of gyrogenesis may underlie the formation of the first major folds during the early stage of radial growth of the cerebral cortex (Hasnain et al. 2001, 2006). Neurons migrate tangentially at later stages of corticogenesis (Rakic 1990). A mechanical folding model based on the differential tangential growth of the inner and outer cortical layers has been proposed for these stages (Richman et al. 1975). The formation of secondary and tertiary sulci may be influenced by this mechanical folding and other chaotic events (Hasnain et al. 2001, 2006). In summary, the early major folds appear to show greater spatial invariance during development as they deepen and have a stronger spatial covariance with functional areas under closer genetic control than later developing sulci. The apparent immobility of the sulcal fundi has been reported (Smart and McSherry 1986) and reproduced using a simulated morphogenetic model (Toro and Burnod 2005). With regard to the high-frequency sulcal pit regions in our study, it appears that the first major folds develop and deepen at similar positions between individuals and retain their identity without

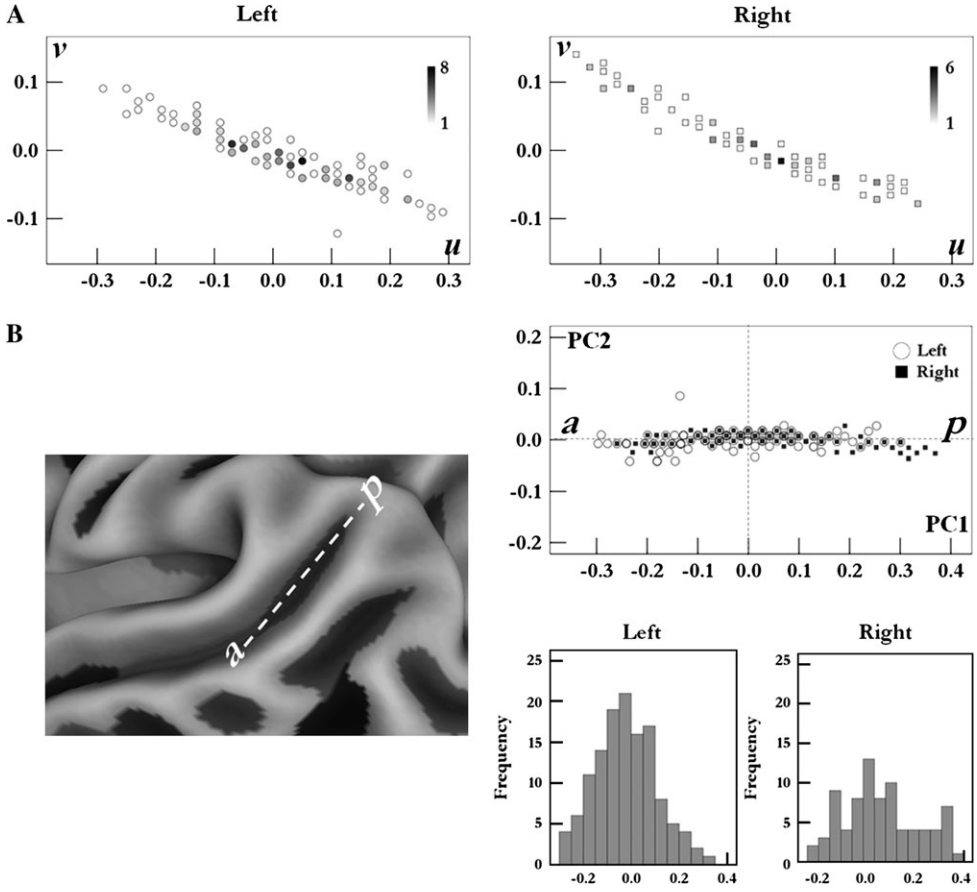

Figure 7. Scatter plots of sulcal pits in the left and right STS *d* on the *u* and *v* coordinate systems (*A*), a scatter plot showing the distribution of sulcal pits on the 2 axes of a PCA, and histograms for the data projected onto the first component (*B*). The scale indicates the number of sulcal pits mapped on the same position. The spatial variance of the pits in the right hemisphere is greater than that in the left hemisphere.

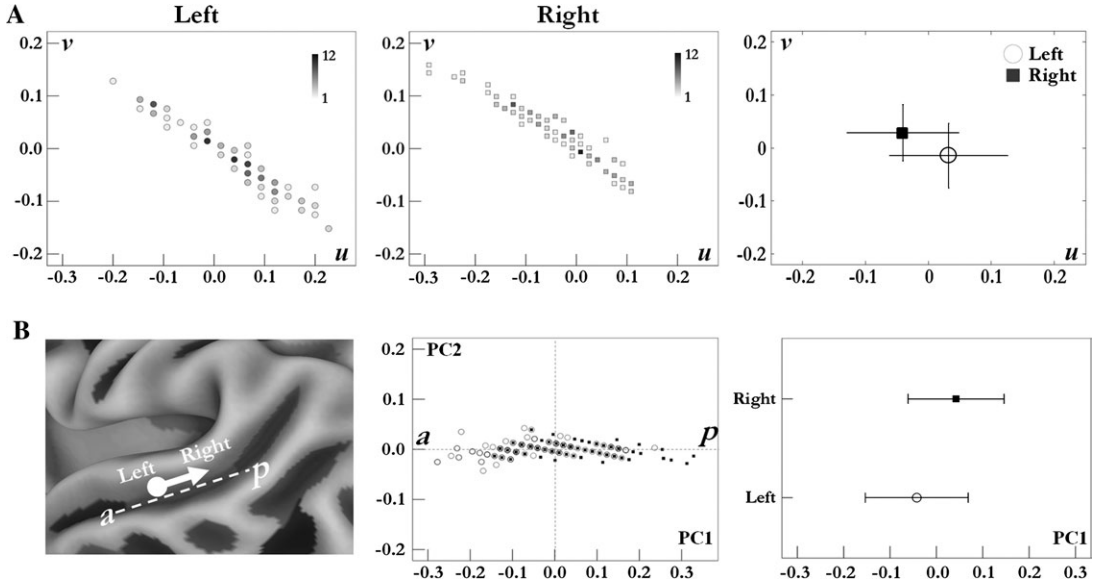

Figure 8. Scatter plots with 2D error bars for sulcal pits in the left and right STS *c* on the *u* and *v* coordinate systems (*A*), a scatter plot showing the distribution of sulcal pits on the 2 axes of a PCA, and error bars for the data projected onto the first component (*B*). The scale indicates the number of sulcal pits mapped onto the same position. The error bar represents the mean and the standard deviation. The positional difference in the distribution of the pits between the left and right hemispheres is shown. The sulcal pits in the left STS *c* are distributed in a more anterior region along the sulcal line compared with those in the right.

merging into other folds. They develop from consistently predetermined and spatially stable functional areas arising from the protomap and powerful gyrogenesis in those areas at an early stage. We suggest that the ontogenetic protomaps of high-frequency regions might generally resemble each other more than those for other regions in human brains.

Most sulci contained just 1 or 2 sulcal pit clusters showing a high frequency of more than 90%. We suggest that many sulci develop with 1 or 2 of the early major folds. For example, the major pit cluster in the CiS was present only in the posterior region (CiS *f*, with 99% frequency in both hemispheres). Other regions that have a low frequency may have variations in regard to the number and location of the first sulcal folds. Alternatively, sulcal pits may disappear during brain development because of the intricate merging of the first folds. There is a possibility that imperfections in our method may miss true sulcal pits. More than 70% of sulcal pits were localized within a 5 mm radius of the densest point in some of the high-frequency clusters. The sulcal pits in the clusters with high density and focal spatial localization (left IPS *b*, right MFS *a* and PoCS *b*, and both (left and right) the junction between SFS and PrCS, the junction between PrCS and IFS, CS *b*, CoS *b*, and SPS) appear to be useful as stable anatomical landmarks for improving current brain-image registration and cortical pattern matching.

Hemispheric Asymmetries in the Frequency and the Spatial Distribution of Sulcal Pits

We found hemispheric asymmetries in the frequency and distribution of sulcal pits. Because deep, early sulcal pits appear to be closely related to functional areas and under genetic control, the asymmetric distribution of sulcal pits may be associated with asymmetric genetic programs and functional hemispheric lateralization. The most statistically significant and interesting asymmetries were shown in the STS. For a better insight, we performed a principal component analysis (PCA) of the sulcal pit data on the local coordinate system and plotted them using the 2 axes of the PCA. The first component explained almost all variation of the sulcal pits in the STS *c* and *d* because the STS is an elongate sulcus and the distribution of sulcal pits is along the sulcal line (Figs 7*B* and 8*B*). We constructed histograms using the data projected onto the first component and confirmed the difference between the left and right hemispheres in the spatial variance of the pits in the STS *d* (Fig. 7*B*). This difference was statistically significant when an equality of variance was assessed using Levene's test ($F_{1,207}$ = 8.59, P = 0.0038). The sulcal pits in the left STS *c* distributed in a more anterior region along the sulcal line compared with those in the right (Fig. 8*B*). A paired *t* test using the data of the first component showed that the positional asymmetry of the pits in the STS *c* is statistically significant (t = 7.66, P < 0.0001).

The specialization of the left hemisphere for language is one of the earliest and the best-known functional asymmetries. Cortical activation associated with language processing was strongly lateralized to the left superior temporal gyrus (STG) in functional MRI and positron emission topography studies (Karbe et al. 1995; Binder et al. 1997; Schlosser et al. 1998; Tzourio et al. 1998; Balsamo et al. 2002; Bleich-Cohen et al. 2009). In relation to functional asymmetry, structural asymmetries in the STS and its nearby areas (Heschl's gyrus and planum temporale) have been reported (Witelson and Pallie 1973; Penhune et al. 1996; Steinmetz 1996; Good et al. 2001; Watkins et al. 2001; Sowell et al. 2002; Emmorey et al. 2003). The regions of the STS *c* and *d* clusters are part of Wernicke's area and the STG is their neighboring gyrus. We suggest that the higher frequency and smaller spatial variance of sulcal pits in the left STS *d* may be related to the lateralization of language function to the left hemisphere, developing more consistently and strongly than for the right hemisphere. We showed that sulcal pits in the left STS *c* were located in a more anterior region. Larger functional area and cortical structure for language processing in the left hemisphere may result in the different position of first folds between the left and right hemispheres. The present study cannot fully address whether the asymmetry of sulcal pits is a key biomarker of the lateralization of the language function. The relationship between the positional and frequency asymmetry of sulcal pits, and functional and structural asymmetries should be further investigated in future work.

The sulcal pattern analysis in the STS showed that the *plis de passage* in the intermediate region of the STS was never superficial on the right side and was much more visible on the left (Ochiai et al. 2004). Because the region of intermediate *plis de passage* looks like the boundary between the STS *b* and *c*, the significantly higher frequency in the left STS *b* that we found is directly related to the previous result of more superficial left intermediate *plis de passage*. The difference in pit frequency between the hemispheres may be related to the asymmetry in sulcal development. The STS *b* cluster in the right hemisphere was not included in the original cluster map because of the low frequency and density of sulcal pits. The STS had 3 pit clusters in the right hemisphere, but 4 clusters in the left (Fig. 6). In a previous atlas of the sulci (Ono et al. 1990), the STS was described as being continuous in a third of cases (36% on the left and 28% on the right). The STS was divided into 2 segments in 48% on the right and 32% on the left, into 3 segments in 16% on the right and 16% on the left, and into 4 segments but in only 24% of cases on the left. Our observation of only 3 pit clusters in the right STS is consistent with the lack of division of the STS into more than 4 segments in the right hemisphere. Up to the end of the first postnatal year, the left language regions, including the STS, lag behind the right side in development, perhaps to await speech development (Chi et al. 1977; Toga and Thompson 2003). A recent neuroimaging study in preterm newborns demonstrated that gyral complexity is present in the right STS earlier than in the left (Dubois et al. 2008). In adults, the STS is significantly deeper in the right hemisphere than in the left (Ochiai et al. 2004; Van Essen 2005). We suggest that the first folds formed in the right STS usually appear earlier near the pit of STS *c*, and then develop into a large sulcal segment or perhaps merge with neighboring folds, resulting in greater depth than for the left STS. Finally, there are fewer than 4 sulcal segments in the right STS (Ono et al. 1990) because of prominent and deep folding in the region of STS *c* and variations in the development of the STS *b* and *d* areas. Although the development of the STS in the left hemisphere lags behind that of the right, fold formation in the STS *c* region may proceed with neighboring folds, preserving their identity more consistently than on the right side, resulting in the frequent appearance of 4 segments in the left STS (Ono et al. 1990).

As in the STS, the frequency of sulcal pits in the PoCS *a* was significantly greater in the left than in the right hemisphere. Previous structural analysis of the somatosensory area showed

the same trend in leftward asymmetry. The area of the left postcentral gyrus significantly exceeded that of the right (Jung et al. 2003). The maturation of the somatosensory fibers was analyzed in infants, and the asymmetry in myelination favoring the left side has been described (Dubois et al. 2009). Higher fractional anisotropy in the left anterior part of the CaS was also shown compared with the right (Dubois et al. 2009). We found that the left anterior CaS (CaS *a*) had a statistically significant higher frequency of sulcal pits.

Hemispheric Spatial Covariance of Sulcal Pits

Our finding that the left and right sulcal pits are spatially covariant in the clusters in the 4 major sulci (CS *b*, SF, CaS *a*, and POS *a*) is highly significant. In a previous study investigating the early sulcal emergence in vivo, the interhemispheric fissure, SF, callosal sulcus, POS, CaS, CiS, and CS were the first to be identified in preterm newborns (Dubois et al. 2008). It is worthy of note that all the significant clusters in our spatial covariance analysis belong to the earliest developed sulci. It might provide clues for the developmental process of sulcal folds in the human brain. However, further studies should be performed to clarify its biological meaning.

Conclusions

We generated a group map on a surface template showing the intrinsic variability of sulcal pits clustered in specific focal areas, with a relatively consistent pattern of spatial distribution between subjects. The sulcal pits were automatically extracted from the cortical surface using a robust methodological procedure. Our analyses of sulcal pit distribution and its asymmetric pattern support previous empirical and theoretical studies, and provide additional insights concerning the anatomical and functional development of the brain.

Funding

Korea Science and Engineering Foundation (KOSEF) NRL program grant funded by the Korea government (MEST) (grant number R0A-2007-000-20068-0).

Notes

Conflict of Interest: None declared.

Address correspondence to Jong-Min Lee, PhD, Department of Biomedical Engineering, Hanyang University, P.O. Box 55, Sungdong, Seoul 133-605, South Korea. Email: ljm@hanyang.ac.kr.

References

Balsamo LM, Xu B, Grandin CB, Petrella JR, Braniecki SH, Elliott TK, Gaillard WD. 2002. A functional magnetic resonance imaging study of left hemisphere language dominance in children. Arch Neurol. 59:1168–1174.

Binder JR, Frost JA, Hammeke TA, Cox RW, Rao SM, Prieto T. 1997. Human brain language areas identified by functional magnetic resonance imaging. J Neurosci. 17:353–362.

Bleich-Cohen M, Hendler T, Kotler M, Strous RD. 2009. Reduced language lateralization in first-episode schizophrenia: an fMRI index of functional asymmetry. Psychiatry Res. 171:82–93.

Cachia A, Mangin JF, Riviere D, Kherif F, Boddaert N, Andrade A, Papadopoulos-Orfanos D, Poline JB, Bloch I, Zilbovicius M, et al. 2003. A primal sketch of the cortex mean curvature: a morphogenesis based approach to study the variability of the folding patterns. IEEE Trans Med Imaging. 22:754–765.

Chi JG, Dooling EC, Gilles FH. 1977. Left-right asymmetries of the temporal speech areas of the human fetus. Arch Neurol. 34:346–348.

Chung MK, Worsley KJ, Robbins S, Paus T, Taylor J, Giedd JN, Rapoport JL, Evans AC. 2003. Deformation-based surface morphometry applied to gray matter deformation. Neuroimage. 18:198–213.

Collins DL, Neelin P, Peters TM, Evans AC. 1994. Automatic 3D intersubject registration of MR volumetric data in standardized Talairach space. J Comput Assist Tomogr. 18:192–205.

Cunningham DJ. 1905. Text-book of anatomy. New York: W. Wood and Company.

Dubois J, Benders M, Cachia A, Lazeyras F, Ha-Vinh Leuchter R, Sizonenko SV, Borradori-Tolsa C, Mangin JF, Huppi PS. 2008. Mapping the early cortical folding process in the preterm newborn brain. Cereb Cortex. 18:1444–1454.

Dubois J, Hertz-Pannier L, Cachia A, Mangin JF, Le Bihan D, Dehaene-Lambertz G. 2009. Structural asymmetries in the infant language and sensori-motor networks. Cereb Cortex. 19:414–423.

Duvernoy DM. 1991. The human brain: surface, three-dimensional sectional anatomy and MRI. New York: Springer-Verlag.

Emmorey K, Allen JS, Bruss J, Schenker N, Damasio H. 2003. A morphometric analysis of auditory brain regions in congenitally deaf adults. Proc Natl Acad Sci USA. 100:10049–10054.

Fukuchi-Shimogori T, Grove EA. 2001. Neocortex patterning by the secreted signaling molecule FGF8. Science. 294:1071–1074.

Geschwind DH, Miller BL. 2001. Molecular approaches to cerebral laterality: development and neurodegeneration. Am J Med Genet. 101:370–381.

Good CD, Johnsrude I, Ashburner J, Henson RN, Friston KJ, Frackowiak RS. 2001. Cerebral asymmetry and the effects of sex and handedness on brain structure: a voxel-based morphometric analysis of 465 normal adult human brains. Neuroimage. 14:685–700.

Gratiolet LP. 1854. Mémoire sur les Plis Cérébraux de l"Homme et des Primates. Paris: Bertrand.

Hasnain MK, Fox PT, Woldorff MG. 2001. Structure-function spatial covariance in the human visual cortex. Cereb Cortex. 11:702–716.

Hasnain MK, Fox PT, Woldorff MG. 2006. Hemispheric asymmetry of sulcus-function correspondence: quantization and developmental implications. Hum Brain Mapp. 27:277–287.

Im K, Lee JM, Lyttelton O, Kim SH, Evans AC, Kim SI. 2008a. Brain size and cortical structure in the adult human brain. Cereb Cortex. 18:2181–2191.

Im K, Lee JM, Seo SW, Kim SH, Kim SI, Na DL. 2008b. Sulcal morphology changes and their relationship with cortical thickness and gyral white matter volume in mild cognitive impairment and Alzheimer's disease. Neuroimage. 43:103–113.

Jung P, Baumgartner U, Bauermann T, Magerl W, Gawehn J, Stoeter P, Treede RD. 2003. Asymmetry in the human primary somatosensory cortex and handedness. Neuroimage. 19:913–923.

Karbe H, Wurker M, Herholz K, Ghaemi M, Pietrzyk U, Kessler J, Heiss WD. 1995. Planum temporale and Brodmann's area 22. Magnetic resonance imaging and high-resolution positron emission tomography demonstrate functional left-right asymmetry. Arch Neurol. 52:869–874.

Kim JS, Singh V, Lee JK, Lerch J, Ad-Dab'bagh Y, Macdonald D, Lee JM, Kim SI, Evans AC. 2005. Automated 3-D extraction and evaluation of the inner and outer cortical surfaces using a Laplacian map and partial volume effect classification. Neuroimage. 27:210–221.

Lanthier M, Maheshari A, Sack J-R. 2001. Approximating shortest paths on weighted polyhedral surfaces. Algorithmica. 30:527–562.

Levene H. 1960. Contributions to Probability and Statistics: Essays in Honor of Harold Hotelling. Stanford: Stanford University Press. p. 278–292.

Lohmann G, von Cramon DY, Steinmetz H. 1999. Sulcal variability of twins. Cereb Cortex. 9:754–763.

Lohmann G, von Cramon DY. 2000. Automatic labelling of the human cortical surface using sulcal basins. Med Image Anal. 4:179–188.

Lohmann G, von Cramon DY, Colchester AC. 2008. Deep sulcal landmarks provide an organizing framework for human cortical folding. Cereb Cortex. 18:1415–1420.

Lyttelton O, Boucher M, Robbins S, Evans A. 2007. An unbiased iterative group registration template for cortical surface analysis. Neuroimage. 34:1535–1544.

MacDonald D, Kabani N, Avis D, Evans AC. 2000. Automated 3-D extraction of inner and outer surfaces of cerebral cortex from MRI. Neuroimage. 12:340–356.

Mazziotta JC, Toga AW, Evans A, Fox P, Lancaster J. 1995. A probabilistic atlas of the human brain: theory and rationale for its development. The International Consortium for Brain Mapping (ICBM). Neuroimage. 2:89–101.
Meyer M, Desbrun M, Schroder P, Barr AH. 2002. Discrete differential-geometry operators for triangulated 2-manifolds. VisMath. 35–58.
Miyashita-Lin EM, Hevner R, Wassarman KM, Martinez S, Rubenstein JL. 1999. Early neocortical regionalization in the absence of thalamic innervation. Science. 285:906–909.
Ochiai T, Grimault S, Scavarda D, Roch G, Hori T, Riviere D, Mangin JF, Regis J. 2004. Sulcal pattern and morphology of the superior temporal sulcus. Neuroimage. 22:706–719.
Ono M, Kubik S, Abernathey CD. 1990. Atlas of the Cerebral Sulci. Stuttgart, New York: Georg Thieme Verlag.
Penhune VB, Zatorre RJ, MacDonald JD, Evans AC. 1996. Interhemispheric anatomical differences in human primary auditory cortex: probabilistic mapping and volume measurement from magnetic resonance scans. Cereb Cortex. 6:661–672.
Piao X, Hill RS, Bodell A, Chang BS, Basel-Vanagaite L, Straussberg R, Dobyns WB, Qasrawi B, Winter RM, Innes AM, et al. 2004. G protein-coupled receptor-dependent development of human frontal cortex. Science. 303:2033–2036.
Rakic P. 1988. Specification of cerebral cortical areas. Science. 241:170–176.
Rakic P. 1990. Principles of neural cell migration. Experientia. 46:882–891.
Rakic P. 2001. Neurobiology. Neurocreationism—making new cortical maps. Science. 294:1011–1012.
Rakic P. 2004. Neuroscience. Genetic control of cortical convolutions. Science. 303:1983–1984.
Rao A, Aljabar P, Rueckert D. 2008. Hierarchical statistical shape analysis and prediction of sub-cortical brain structures. Med Image Anal. 12:55–68.
Regis J, Mangin JF, Frouin V, Sastre F, Peragut JC, Samson Y. 1995. Generic model for the localization of the cerebral cortex and preoperative multimodal integration in epilepsy surgery. Stereotact Funct Neurosurg. 65:72–80.
Regis J, Mangin JF, Ochiai T, Frouin V, Riviere D, Cachia A, Tamura M, Samson Y. 2005. Sulcal root" generic model: a hypothesis to overcome the variability of the human cortex folding patterns. Neurol Med Chir (Tokyo). 45:1–17.
Rettmann ME, Han X, Xu C, Prince JL. 2002. Automated sulcal segmentation using watersheds on the cortical surface. Neuroimage. 15:329–344.
Richman DP, Stewart RM, Hutchinson JW, Caviness VS, Jr. 1975. Mechanical model of brain convolutional development. Science. 189:18–21.
Riss W. 1984. Testing a theory of brain function by computer methods. III. Detecting cerebral asymmetry in normal adults. Brain Behav Evol. 24:13–20.
Robbins S. 2003. Anatomical Standardization of the Human Brain in Euclidean 3-space and on the Cortical 2-Manifold. PhD Thesis. McGill University. Montreal, Que., Canada: School of Computer Science.
Robbins S, Evans AC, Collins DL, Whitesides S. 2004. Tuning and comparing spatial normalization methods. Med Image Anal. 8:311–323.
Rubenstein JL, Rakic P. 1999. Genetic control of cortical development. Cereb Cortex. 9:521–523.
Schlosser MJ, Aoyagi N, Fulbright RK, Gore JC, McCarthy G. 1998. Functional MRI studies of auditory comprehension. Hum Brain Mapp. 6:1–13.
Sled JG, Zijdenbos AP, Evans AC. 1998. A nonparametric method for automatic correction of intensity nonuniformity in MRI data. IEEE Trans Med Imaging. 17:87–97.
Smart IH, McSherry GM. 1986. Gyrus formation in the cerebral cortex in the ferret. I. Description of the external changes. J Anat. 146:141–152.
Sowell ER, Thompson PM, Peterson BS, Mattson SN, Welcome SE, Henkenius AL, Riley EP, Jernigan TL, Toga AW. 2002. Mapping cortical gray matter asymmetry patterns in adolescents with heavy prenatal alcohol exposure. Neuroimage. 17:1807–1819.
Steinmetz H. 1996. Structure, functional and cerebral asymmetry: in vivo morphometry of the planum temporale. Neurosci Biobehav Rev. 20:587–591.
Sun T, Patoine C, Abu-Khalil A, Visvader J, Sum E, Cherry TJ, Orkin SH, Geschwind DH, Walsh CA. 2005. Early asymmetry of gene transcription in embryonic human left and right cerebral cortex. Science. 308:1794–1798.
Sun T, Walsh CA. 2006. Molecular approaches to brain asymmetry and handedness. Nat Rev Neurosci. 7:655–662.
Tao X, Prince JL, Davatzikos C. 2002. Using a statistical shape model to extract sulcal curves on the outer cortex of the human brain. IEEE Trans Med Imaging. 21:513–524.
Toga AW, Thompson PM. 2003. Mapping brain asymmetry. Nat Rev Neurosci. 4:37–48.
Toro R, Burnod Y. 2005. A morphogenetic model for the development of cortical convolutions. Cereb Cortex. 15:1900–1913.
Tzourio N, Crivello F, Mellet E, Nkanga-Ngila B, Mazoyer B. 1998. Functional anatomy of dominance for speech comprehension in left handers vs right handers. Neuroimage. 8:1–16.
Van Essen DC. 2005. A Population-Average, Landmark- and Surface-based (PALS) atlas of human cerebral cortex. Neuroimage. 28:635–662.
Watkins KE, Paus T, Lerch JP, Zijdenbos A, Collins DL, Neelin P, Taylor J, Worsley KJ, Evans AC. 2001. Structural asymmetries in the human brain: a voxel-based statistical analysis of 142 MRI scans. Cereb Cortex. 11:868–877.
Welker W. 1990. Why does cerebral cortex fissure and fold? A review of determinants of gyri and sulci. In: Jones EG, Pertes A, editors. Cerebral cortex. Vol. 8B. New York: Plenum. p. 3–136.
Witelson SF, Pallie W. 1973. Left hemisphere specialization for language in the newborn. Neuroanatomical evidence of asymmetry. Brain. 96:641–646.
Yang F, Kruggel F. 2008. Automatic segmentation of human brain sulci. Med Image Anal. 12:442–451.
Zijdenbos AP, Evans AC, Riahi F, Sled JG, Chui J, Kollakian V. 1996. Automatic quantification of multiple sclerosis lesion volume using stereotaxic space. Proc, 4th Intl Conf on Visualization in BioMed Computing VBC, Lecture Notes in Computer Science. 1131: 439–448.